

The VampPrior Mixture Model

Andrew Stirn¹ David A. Knowles^{1,2}

Abstract

Current clustering priors for deep latent variable models (DLVMs) require defining the number of clusters a-priori and are susceptible to poor initializations. Addressing these deficiencies could greatly benefit deep learning-based scRNA-seq analysis by performing integration and clustering simultaneously. We adapt the VampPrior (Tomczak & Welling, 2018) into a Dirichlet process Gaussian mixture model, resulting in the *VampPrior Mixture Model* (VMM), a novel prior for DLVMs. We propose an inference procedure that alternates between variational inference and Empirical Bayes to cleanly distinguish variational and prior parameters. Using the VMM in a Variational Autoencoder attains highly competitive clustering performance on benchmark datasets. Augmenting scVI (Lopez et al., 2018), a popular scRNA-seq integration method, with the VMM significantly improves its performance and automatically arranges cells into biologically meaningful clusters.

1. Introduction

Extracting meaningful knowledge from complex, high-dimensional data is a central promise of data science across many applied disciplines. A striking example is single-cell RNA sequencing (scRNA-seq), which has become ubiquitous in biomedical research, enabling genome-wide profiling of gene expression in up to millions of single cells in one experiment. However, single-cell datasets increasingly contain many samples collected under different conditions in different laboratories using different methodologies, leading to complex nested batch effects (Luecken et al., 2022) that often drive larger variance than the biological signals of interest. The goal of scRNA-seq integration is to remove these batch effects while conserving biological variation such as cell type identity and disease effects.

¹Department of Computer Science, Columbia University, New York, USA ²New York Genome Center, New York, USA. Correspondence to: Andrew Stirn <andrew.stirn@cs.columbia.edu>, David A. Knowles <daknowles@cs.columbia.edu>.

Preliminary work. Copyright 2024 by the author(s).

The modus operandi of scRNA-seq analysis is to first integrate the data by mapping observed data X , a N cells $\times G$ genes matrix, to a lower dimensional embedding Z , where each of the N cells have $\text{dim}(z_i) \ll G$. Analysis proceeds by further reducing Z to visualizable dimensions with t-SNE (Van der Maaten & Hinton, 2008), UMAP (McInnes et al., 2018), or MDE (Agrawal et al., 2021). These methods are notorious for finding structure where no structure exists (Chari & Pachter, 2023). When the embedding function does not account for systematic shifts in expression profiling between datasets and/or batches that use different scRNA-seq technologies, misleading structure can arise, confounding standard analysis pipelines. Accordingly, Lähnemann et al. (2020) identify atlas-level integration as one of the grand challenges of single-cell data science.

Seurat v3 (Stuart et al., 2019) and Harmony (Korsunsky et al., 2019) are two widely used integration methods that use canonical correlation analysis coupled with mutual nearest neighbors and principal component analysis coupled with k -means, respectively. Luecken et al. (2022) benchmark 12 integration methods on 13 atlas-level integration tasks and find that, while these two methods perform well on smaller scRNA-seq integration tasks, they underperform on more sophisticated atlas-level integrations relative to DLVMs that use amortized variational inference (VI) such as scVI (Lopez et al., 2018) and its derivatives (Svensson et al., 2020; Xu et al., 2021). Harmony iteratively distorts batch-specific embeddings to attempt to align the k -mean clusters across batches, thereby removing batch effects in the embedded space. In contrast, scVI passes both the encoder and decoder a one-hot encoding of the batch identifier to learn a shared, batch effect-free embedding; Section 5 discusses why this works. However, with a fixed $\mathcal{N}(0, I)$ prior on the embedding, scVI's generative process does not explicitly encourage clustering of similar cells. We propose replacing scVI's $\mathcal{N}(0, I)$ prior with a more flexible mixture prior that both improves its integration performance and provides robust clustering capabilities. We anticipate well clustered and integrated embeddings will improve current single-cell analysis pipelines.

To achieve simultaneous integration and clustering we first investigate a method that replaces the $\mathcal{N}(0, I)$ prior of the standard Variational Autoencoder (VAE) (Kingma & Welling, 2013; Rezende et al., 2014) with a Gaussian mix-

ture model (GMM) (Jiang et al., 2017). We extend Jiang et al. (2017)'s approach by placing a VampPrior (Tomczak & Welling, 2018) over the cluster centers, and reformulate the mixture to approximate a Dirichlet process (DP) mixture. We call our prior the *VampPrior Mixture Model* (VMM). Unlike Jiang et al. (2017), the VMM requires no pre-training and automatically discovers an appropriate number of clusters. Jiang et al. (2017) and Tomczak & Welling (2018) jointly optimize variational and prior parameters. Instead, we alternate amortized VI steps (fitting variational parameters with fixed prior parameters) with Empirical Bayes steps (fitting just prior parameters).

Since the VMM merely replaces a $\mathcal{N}(0, I)$ prior, it is applicable to any DLVM with continuous variables. Section 4 employs a VMM within the VAE's generative process for image clustering. The VMM not only outperforms VAE-based clustering methods but also approaches state-of-the-art unsupervised classification performance. Section 5 integrates the VMM into scVI and finds significant improvements to both batch correction and biological conservation during scRNA-seq integration. The group behind scVI has developed numerous other DLVMs for scRNA-seq, scATAC-seq, multimodal single-cell, and spatial transcriptomic data analyses that all use $\mathcal{N}(0, I)$ priors in their generative processes. Integrating the VMM into these tools and many others would be straightforward, further amplifying this work's potential impact.

2. Background

This section briefly reviews relevant background material.

2.1. The Variational Autoencoder

DLVMs are a class of generative models that parameterize the likelihood of observed variables with neural networks operating on latent variables. The VAE (Kingma & Welling, 2013) is a DLVM with the following generative process:

$$z_i \sim \mathcal{N}(0, I) \quad \forall i \in [N] \quad (1)$$

$$x_i|z_i \sim p_\theta(x_i|z_i) \triangleq p(x_i|f(z_i; \theta)) \quad \forall i \in [N], \quad (2)$$

where f is the decoding neural network with parameters θ . The VAE employs amortized VI by defining the variational family $q_\phi(z_i; x_i) \triangleq \mathcal{N}(z_i; g(x_i; \phi))$, where g is the encoding neural network with parameters ϕ , specifying both mean and covariance. Inference maximizes the evidence lower bound (ELBO),

$$\mathcal{L}(\mathcal{D}; \theta, \phi) = \sum_{x \in \mathcal{D}} \mathbb{E}_{q_\phi(z|x)} [\log p_\theta(x|z)] - \text{KL}(q_\phi(z|x)||p(z)), \quad (3)$$

w.r.t. θ and ϕ using black-box VI (Ranganath et al., 2014) and reparameterization gradients (Williams, 1992).

2.2. The VampPrior

Tomczak & Welling (2018) identify the prior that maximizes the VAE's ELBO (3) as the aggregate posterior $p^*(z) = N^{-1} \sum_{i=1}^N q_\phi(z_i; x_i)$, taken over the N training points. They replace the VAE's prior (1) with

$$p(z) \triangleq \frac{1}{K} \sum_{j=1}^K q(z; g(u_j, \phi)),$$

where pseudo-inputs u_1, \dots, u_K are trainable prior parameters initialized with $K \ll N$ randomly selected (without replacement) training points for efficiency. Inference proceeds by maximizing (3) w.r.t. θ , ϕ , and u .

2.3. Gaussian Mixture Models

A GMM on z can be represented as,

$$z_1, \dots, z_N | \pi, \mu, \Lambda \sim \sum_{j=1}^K \pi_j \mathcal{N}(z|\mu_j, \Lambda_j^{-1}) \quad (4)$$

with mixing proportions π , cluster means μ , and cluster precisions Λ . In a Bayesian framework, we place priors on all parameters,

$$\alpha \sim \text{InverseGamma}(1, 1) \quad (5)$$

$$\pi | \alpha \sim \text{Dirichlet}(\alpha K^{-1} \mathbf{1}_K^T) \quad (6)$$

$$\mu_1, \dots, \mu_K \stackrel{\text{i.i.d.}}{\sim} \mathcal{N}(0, I) \quad (7)$$

$$\Lambda_1, \dots, \Lambda_K \stackrel{\text{i.i.d.}}{\sim} \text{Wishart}\left(p+2, \frac{K^{\frac{1}{p}}}{p+2} I\right), \quad (8)$$

where $p \equiv \dim(z)$. Taking $K \rightarrow \infty$ results in a DP GMM (Edward, 2000). In addition, Ishwaran & James (2002) prove that an upper bound for the absolute difference between the marginal densities of a K -component GMM and the ∞ -component GMM integrated over \mathbb{R}^p decays exponentially w.r.t. K . Thus, our GMM with sufficiently large K set a-priori will approximate the limiting DP GMM well.

3. The VampPrior Mixture Model

Before introducing the VMM, we first show how to use (4)-(8) as a hierarchical prior that replaces (1) in the VAE. From there, we develop our inference algorithm that alternates between VI and Empirical Bayes steps. From there, switching to the VMM is a straightforward change to (7).

3.1. A Dirichlet Process GMM Prior

Fraley & Raftery (2007) recommend Wishart parameters for GMMs with observed z_i 's. In our setting, z_i 's are latent, so we replace the empirical precision term in the Wishart's

Algorithm 1 Alternating VI and Empirical Bayes Steps

while not converged **do**

 Sample batch: $\mathcal{B} \leftarrow \{x_1, \dots, x_M \sim \hat{\Pr}(\mathcal{D})\}$
 VAE inference: $(\phi, \theta) \leftarrow (\phi, \theta) + \gamma_1 \nabla_{\phi, \theta} \mathcal{L}(\mathcal{B}; \theta, \phi)$
 Sample approx. posterior: $z_i \sim q_\phi(z_i; x_i) \quad \forall i \in [M]$
 Prior EM: $\psi \leftarrow \psi + \gamma_2 \nabla_\psi \mathbb{E}_{q(c)} [\log p(z, c, \pi, \mu, \Lambda, \alpha)]$
end while

scale matrix with the identity. We found that further normalizing their scale matrix by $p+2$ to ensure $\mathbb{E}[\Lambda_j] = K^{\frac{1}{p}} I$ makes (8) more tolerant to different $p \equiv \dim(z)$'s.

For a VAE, defining $p(z)$ as a GMM changes only the Kullback–Leibler (KL) divergence term in (3) to

$$\text{KL} \left(q_\phi(z; x) \middle\| \sum_{j=1}^K \pi_j \mathcal{N}(z|\mu_j, \Lambda_j^{-1}) \right). \quad (9)$$

3.2. Alternating Inference Algorithm

We use a GMM prior to achieve a clustered latent representation; this, however, requires fitting the GMM parameters. To avoid ambiguities that occur when mixing variational and prior inference, such as Tomczak & Welling (2018) fitting ϕ both as a variational and prior parameter, we propose cleanly partitioning the variational and prior parameters and corresponding inference procedures. We treat θ and ϕ exclusively as variational parameters and $\alpha, \pi, \mu, \Lambda$ as prior parameters¹. We perform VI (optimizing (3) w.r.t. θ and ϕ) to fit variational parameters and perform maximum a posteriori (MAP) (optimizing (4)–(8) w.r.t. to $\psi \triangleq \{\alpha, \pi, \mu, \Lambda\}$) to fit prior parameters. Algorithm 1 shows how we alternate between these two separate inference procedures.

In the first two lines, we perform stochastic amortized VI for the VAE as usual. We then (approximately) sample the aggregate posterior and perform gradient based MAP via expectation maximization (EM), learning point estimates for $\alpha, \pi, \mu, \Lambda$. Section 3.3 discusses our choice for using MAP as opposed to VI. EM represents the GMM as

$$c_i | \pi \sim \text{Categorical}(\pi), \quad z_i | c_i, \mu, \Lambda \sim \mathcal{N}(z|\mu_{c_i}, \Lambda_{c_i}^{-1})$$

and sets $q(c_i = j) \propto \log p(z_i | c_i = j, \mu, \Lambda) + \log \pi_j$.

Unlike the standard VAE, the GMM prior has local and global parameters. Sampling a batch of M z_i 's up-weights the prior's contribution by NM^{-1} , which we found to be beneficial. Rather than tuning (5), (7), and (8)'s multiple parameters to balance the likelihood and prior, one can simply adjust M , relying on the Bayesian paradigm that having more (fewer) data decreases (increases) the prior's influ-

¹Direct optimization of θ can be viewed as part of VI by considering a uniform prior and defining $q(\theta)$ as a Dirac delta.

ence. Applications with specific batch size requirements can adjust the prior parameters directly.

3.3. The VMM Prior

Our VampPrior mixture model changes (7) to

$$\mu_j \sim q_\phi(\mu_j; u_j) \quad \forall j \in [K], \quad (10)$$

which requires modifying (9) to

$$\text{KL} \left(q_\phi(z; x) \middle\| \sum_{j=1}^K \pi_j \mathbb{E}_{q_\phi(\mu_j; u_j)} [\mathcal{N}(z|\mu_j, \Lambda_j^{-1})] \right) \quad (11)$$

during VAE inference. We integrate the expectation analytically to compute the predictive component distributions.

While the GMM finds point estimates for μ_1, \dots, μ_K , the VMM fits their distributional parameters, pseudo-inputs u_1, \dots, u_K , analogous to the VampPrior. Following Tomczak & Welling (2018), we initialize pseudo-inputs with randomly sampled training data. After replacing μ with u in prior parameter set ψ , Algorithm 1 adjusts nicely to the VMM, requiring only that the E-step now also be w.r.t. $q_\phi(\mu; u)$ (the joint distribution for μ_1, \dots, μ_K):

$$\mathbb{E}_{q(c)q_\phi(\mu; u)} [\log p(z, c, \pi, \mu, \Lambda, \alpha)],$$

which we again integrate analytically. The M-step then back propagates through $g(u_j; \phi)$, treating ϕ as a constant, to compute gradients w.r.t. u_j . Thus, we treat ϕ exclusively as a variational parameter unlike Tomczak & Welling (2018).

Using VI instead of MAP EM for prior inference would suggest selecting a Wishart distribution for $q(\Lambda_j)$. In this case, $\mathbb{E}_{q_\phi(\mu_j; u_j)q(\Lambda_j)} [\log \mathcal{N}(z|\mu_j, \Lambda_j^{-1})]$, a term in the resulting ELBO, admits analytic integration. However, the predictive component distribution $\mathbb{E}_{q_\phi(\mu_j; u_j)q(\Lambda_j)} [\mathcal{N}(z|\mu_j, \Lambda_j^{-1})]$ (to replace that in (11)) does not, requiring a Normal-Wishart $q(\mu_j, \Lambda_j)$. Such a change would force us to abandon the VampPrior in (10) and redefine the VAE. However, we want to preserve the VAE modeling choices, changing only $p(z)$ from $\mathcal{N}(0, I)$ to our VMM.

Consider prior selection as a spectrum with the unimodal $\mathcal{N}(0, I)$ prior at one extreme and the exact VampPrior with a mode for each data point at the other. Our DP GMM and VMM are somewhere in the middle between these extremes, and the DP mixture in particular will identify an appropriate number of modes. In the limit of a single cluster, the GMM is equivalent to the unimodal $\mathcal{N}(0, I)$ prior. In the limit of N clusters (or K for the approximate VampPrior), the VMM is equivalent to the VampPrior.

3.4. Comparison with Related Work

Zhou et al. (2022) survey and taxonomize various deep

clustering approaches. Here, we restrict discussion to VAE-based methods that preserve generative capabilities.

The Structured VAE (SVAE) (Johnson et al., 2016) is a general and elegant framework for fitting graphical models with neural networks. They fit a VAE with a latent GMM prior. However, their use of natural gradients requires conditionally conjugate models, limiting their adaptation to scRNA-seq integration methods where zero-inflated distributions are popular modelling choices². We therefore exclude SVAE from our experiments.

The DLGMM (Nalisnick et al., 2016) defines a GMM prior (4) with just a Dirichlet prior (6). They fix the K component means (as equally spaced points on the line) and variances (to one) to encourage similar x_i to gather around one of these preset clusters. They have $q_\phi(z_{ij}; x_i)$ for $j \in [K]$, which requires evaluating the decoder K times and averaging the result according to $\pi_i \sim q_\phi(\pi_i; x_i)$, a Kumaraswamy stick-breaking variational family (Nalisnick & Smyth, 2017). Stirn et al. (2019) show this construction is non-exchangeable and thereby has limited approximation capacity. We attempted to scale their approach beyond one-dimensional z_i 's with limited success and therefore exclude the DLGMM from our experiments.

The GMVAE (Dilokthanakul et al., 2016) defines

$$\begin{aligned} z_i &\sim \mathcal{N}(0, I), & c_i &\sim \text{Categorical}(\pi), \\ y_i|z_i, c_i &\sim \mathcal{N}(f_{c_i}(z_i; \theta_{c_i})), & x_i|y_i &\sim p(x_i; f_x(y_i; \theta_x)) \end{aligned}$$

as its generative process for observed x_i , utilizing K decoders (f_1, \dots, f_K). Their chosen variational family $q(z_i, y_i, c_i) \triangleq q(z_i; g_z(x_i; \phi_z))q(y_i; g_y(x_i; \phi_y))q(c_i|z_i, y_i)$ sets $q(c_i|z_i, y_i)$ to the true posterior. Given their computational complexity, we rely on their reported performance.

VaDE (Jiang et al., 2017) is closest to our proposals. They optimize a GMM for the VAE's $p(z)$:

$$c_i \sim \text{Categorical}(\pi), \quad z_i|c_i \sim \mathcal{N}(\mu_{c_i}, \Sigma_{c_i}).$$

They define $q(c_i; x_i)$ as we do in our E-step and $q_\phi(z_i; x_i)$ in the usual way and optimize their ELBO w.r.t. both variational and prior parameters. For small K fixed a-priori in the non-Bayesian setting, VaDE cannot automatically discover an appropriate number of clusters (as our DP GMM and VMM do) and is highly susceptible to poor initializations, which requires pre-training a deterministic auto-encoder, fitting a GMM to the latent space and using those parameters to initialize VaDE's parameters. Both our GMM and VMM do not require pre-training.

²Zero-inflated distributions model the inability of scRNA-seq to provide complete transcriptomic information due the small amount of RNA within a single cell and incomplete capture.

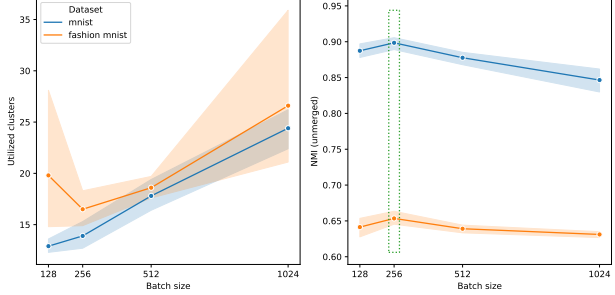


Figure 1: VMM cluster utilization and NMI performance for different batch sizes. Shading denotes 95% CIs. The dotted green rectangle marks the peak NMI performance between class labels and unmerged (i.e. raw) cluster predictions.

4. VAE Experiments

While our intended application is scRNA-seq integration, we first test our methods on the familiar MNIST and Fashion MNIST datasets. We rescale images to $[-1, 1]$, set (2) to $\mathcal{N}(x_i|f(z_i; \theta), \sigma^2 I)$, and fit σ^2 during VAE inference. Following Jiang et al. (2017), we use a three-layer MLP with hidden dimensions [500, 500, 2000] for the encoder and the reverse for the decoder, but anecdotally report that our methods had strong clustering performance for both smaller MLPs and small CNNs. Our variational $q(z; g(x; \phi))$ has full rank covariance. We set $K = 10$ for VaDE (as they do) and $K = 100$ for the VampPrior, our GMM, and the VMM. Reported results average over 10 different trials. Within each trial, data folds and neural network initializations are identical for all methods. Appendix B contains additional details.

4.1. Using the Batch Size to Tune the Prior

Figure 1 shows how adjusting the batch size serves as a proxy for adjusting the DP's concentration. For various batch size settings, we measure how many clusters the VMM discovers $|\{\forall i \in [N] : \arg \max_j q(c_i = j|x_i)\}|$ and the normalized mutual information (NMI) between the true labels and the cluster assignments $\arg \max_j q(c_i = j|x_i)$; as Section 4.3 will explain this penalizes using too many clusters. Increasing the batch size results in the VMM using more clusters as expected since this upweights the likelihood relative to the prior. Since MNIST and Fashion MNIST have the same number of true classes and approximately uniform class distributions, it is reassuring that batch size's effect on cluster utilization is similar and that NMI peaks in both cases with a batch size of 256, which we use for the remainder of this section's experiments.

Table 1: VAE model performance for different priors. We bold top performances using a paired t -test when $p \leq 0.05$.

Prior	$\log p(x x)$	$\log p(x)$	$\mathbb{E}_q[\log p(x z)]$	$\text{KL}(q(z x) p(z))$	$\text{KL}(q(z) p(z))$	$\mathbb{I}[z; n]$
$\mathcal{N}(0, I)$	73.7 ± 2.62	46.9 ± 2.48	59.1 ± 2.98	28 ± 0.15	18.8 ± 0.16	9.21 ± 0.00
VampPrior	215 ± 1.81	165 ± 1.42	197 ± 1.90	50.6 ± 0.46	41.4 ± 0.46	9.21 ± 0.01
Our GMM	80 ± 9.00	53.1 ± 7.88	65.2 ± 8.44	28.1 ± 1.21	18.9 ± 1.21	9.21 ± 0.00
Our VMM	139 ± 9.13	104 ± 7.50	124 ± 8.90	35.2 ± 1.59	25.8 ± 2.19	9.21 ± 0.01

4.2. Model Comparison

Table 1 examines how prior selection affects the VAE’s modeling performance. All columns except the last average over the validation set. We use $\log p(x|x)$ as shorthand to denote the log posterior predictive likelihood:

$$\log \int p_\theta(X^* = x_i|Z) q(Z; g_\phi(x_i)) dZ.$$

The $\log p(x)$ column is the evidence (i.e. log marginal likelihood), which we estimate via importance sampling (Burda et al., 2016). The third and fourth columns are negative distortion and rate (Alemi et al., 2018). Their difference equals the ELBO (3), which indeed lower bounds the measured evidence. The fifth column is the marginal KL divergence (Hoffman & Johnson, 2016) between the aggregate posterior and the prior.

All priors have a similar difference between the evidence and its lower bound. As expected, the VampPrior has the largest ELBO—it is designed to do so—and thereby the largest evidence. However, ELBO maximization often trades large improvements to distortion for small increases in rate. The VampPrior has maximized the ELBO in this way, resulting in the best distortion and worst rate. One may expect the VampPrior to have the smallest marginal KL divergence since it approximates the aggregate posterior $q(z)$. However, rate (fourth column) equals the marginal KL (fifth column) plus a mutual information (MI) term (sixth column) (Hoffman & Johnson, 2016). The MI term has upper-bound $\log N \approx 9.21$ (using validation set size), which we observe for all priors; Hoffman & Johnson (2016) show this is common for non-trivial latent dimensions (e.g. $\dim(z) \geq 10$). Thus, the VampPrior paradoxically has an aggregate posterior furthest from the prior, meaning it is poor at regulating the structure of the learned embedding.

Table 1 shows the VMM has substantially more modelling power than the GMM, despite utilizing the same number of clusters (Table 2). We thus conclude the VMM’s additional modelling performance arises from our choice to integrate the VampPrior into the GMM.

4.3. Clustering Performance

Table 2 compares clustering performance for different models and priors. Because we are in the unsupervised setting, we measure performance on the combined training and val-

idation sets after early stopping on validation set performance (see Appendix B for details). For the unsupervised classification accuracy and NMI (merged) columns, we predict the true label of the cluster’s most probable member for all cluster members; this will merge multiple clusters’ predictions if multiple clusters model the same class. Figure 2 shows the VMM using two clusters to model the two different ways to write the digit 7. In this regime, there is no penalty for the number of clusters—placing an atom on every point achieves perfect scores. In the NMI (unmerged) column, we use the model’s predicted cluster assignments directly in order to punish using too many clusters. We also calculated the Adjusted Rand Index (ARI) and found it had perfect Spearman correlation with NMI in both the merged and unmerged settings, so we report NMI only. We exclude the GMVAE (Dilokthanakul et al., 2016) since their reported results only include accuracy ratios for MNIST, on which they attain 0.778 ± 0.06 for $K = 10$ and 0.928 ± 0.02 for $K = 30$, which are both statistically significantly worse than the VMM.

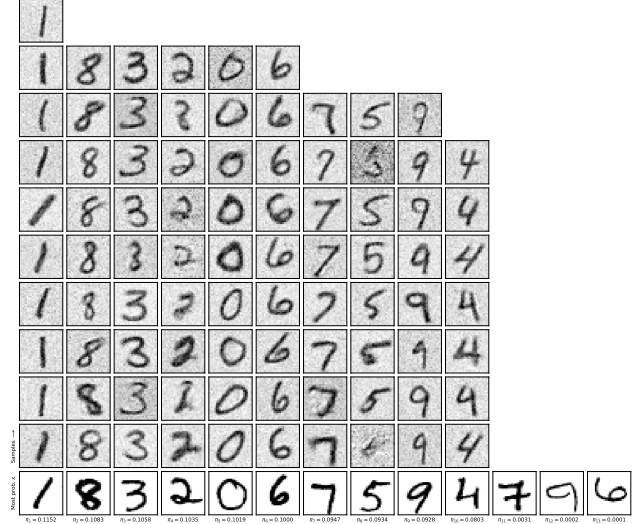


Figure 2: VMM prior predictive samples for MNIST. The number of columns equals the number of utilized clusters. The first row shows the data with the highest probability of belonging to the cluster, under which we print the cluster’s probability π_j . The rows above are samples from the corresponding component distribution. The number of samples for each component equals $\text{round}(10 \cdot \pi_j / \max(\pi))$.

Table 2: Clustering performance for different methods. We bold top performances using a paired t -test when $p \leq 0.05$.

Dataset	mnist w/ dim(z) = 10				fashion mnist w/ dim(z) = 30			
Method	Utilized clusters	Accuracy	NMI (merged)	NMI (unmerged)	Utilized clusters	Accuracy	NMI (merged)	NMI (unmerged)
VampPrior	100 \pm 0.00	0.945 \pm 0.01	0.880 \pm 0.02	0.627 \pm 0.00	100 \pm 0.00	0.775 \pm 0.02	0.691 \pm 0.02	0.529 \pm 0.00
VaDE	10 \pm 0.00	0.857 \pm 0.07	0.838 \pm 0.03	0.832 \pm 0.03	5.5 \pm 2.51	0.352 \pm 0.07	0.496 \pm 0.12	0.499 \pm 0.11
Our GMM	10.7 \pm 2.31	0.902 \pm 0.04	0.878 \pm 0.02	0.876 \pm 0.01	16.1 \pm 3.14	0.513 \pm 0.05	0.516 \pm 0.04	0.509 \pm 0.04
Our VMM	13.9 \pm 2.13	0.960 \pm 0.01	0.907 \pm 0.01	0.899 \pm 0.01	16.5 \pm 2.92	0.712 \pm 0.01	0.688 \pm 0.01	0.653 \pm 0.02

For MNIST, our VMM is the top performer in all categories. For both datasets, our VMM identifies an appropriate number of clusters (knowing there are ten labeled classes) and always has the best unmerged NMI. For Fashion MNIST, the VampPrior has the best accuracy and merged NMI (tied with the VMM), but uses all clusters as it did for MNIST. In contrast, our VMM uses a reasonable number of clusters and has the second-best accuracy for Fashion MNIST as reported by [papers with code](#). The top method there, however, uses 70 latent dimensions compared to our 30. Interestingly, with 70 dimensions, [their MNIST performance](#) is similar to ours despite us using just ten dimensions. Our VaDE implementation’s maximum accuracy ratio of 0.936 on MNIST is nearly identical to their reported value of 0.945, suggesting our implementation is correct. Interestingly, VaDE’s clustering performance does not generalize to Fashion MNIST. We suspect their pre-training procedure failed to provide a good initialization because of higher latent dimensions, Fashion MNIST’s increased heterogeneity, or both. Our DP GMM uses no pre-training and outperforms VaDE on both datasets, confirming the benefit of our choice to approximate a DP mixture with a Bayesian treatment and our partitioned inference procedure. The VMM outperforming our GMM further corroborates the benefit of integrating the VampPrior into the GMM.

Comparing samples from the marginal likelihood (i.e. prior predictive) of a VMM and a VampPrior (Figure 2 and appendix Figure 4), we see that the diversity of samples from the VMM’s cluster components is markedly higher than those from the VampPrior. The VampPrior uses $q_\phi(z; u_j)$ to fully specify a cluster, whereas the VMM uses $q_\phi(\mu; u_j)$ to specify just the cluster’s mean and uses Λ_j to specify its width, affording it the ability to generate more diversity from a single cluster. While diverse, each cluster in the VMM produces semantically similar samples.

5. Single Cell Data Analysis

We now integrate our GMM and VMM into scVI ([Lopez et al., 2018](#)), which models scRNA-seq read counts using a DLVM and amortized VI. For each cell $i \in [N]$ we observe read counts for G genes: $x_i \in \mathbb{N}^G$. Additionally, we observe integer batch (i.e. donor or patient) identifiers s_i for every cell. With observed library sizes computed from x_i (scVI’s

default configuration), scVI models read counts using

$$z_i \sim \mathcal{N}(0, I), \quad x_i | z_i, s_i \sim p(x_i; f_\theta(z_i, s_i)),$$

where $f_\theta(z_i, s_i)$ is a neural network that can parameterize any appropriate distribution for read counts. Matching [Lopez et al. \(2018\)](#)’s supplement and scVI’s documentation, we let f parameterize a zero-inflated negative binomial (ZINB) distribution for all datasets except the lung atlas dataset, for which they [recommend a negative binomial](#). They define the variational family $q_\phi(z_i; x_i, s_i)$ as a normal distribution with diagonal covariance. From a generative modeling perspective, integration seeks a latent representation for biological variation that is disentangled from batch-specific technical variation; that is batch variables serve only as batch-specific calibration factors for the data generating distribution. By giving both the encoder and decoder access to s_i , scVI has no reason to waste z_i ’s limited channel capacity encoding s_i , encouraging it to find a disentangled (i.e. integrated) biological embedding.

Incorporating our DP GMM and VMM into scVI follows Section 3, with one exception for the VMM. Encoder network inputs x_i and s_i are natural numbers and one-hot encoded batch IDs, respectively. Relaxing integer constraints, we transform the first G dimensions (corresponding to x_i) of the VampPrior pseudo-inputs to the positive reals using a softplus and the remaining dimensions (corresponding to one-hot encoded s_i) to the simplex using a softmax.

We use scVI’s API to download the cortex, PBMC, and lung atlas datasets and process them according to [Lopez et al. \(2018\)](#). For each dataset, we use their chosen architecture, latent dimension, and learning rate for amortized VI (γ_1 in Algorithm 1). We tune the batch size and the prior’s learning rate (γ_2 in Algorithm 1) in Appendix C based on the performance of scVI with a VMM prior. Reported results are averages from ten different trials. Within each trial, data folds are identical for all methods and neural network initializations are identical for our scVI implementations.

Table 3 compares the clustering performance of scVI with our GMM and VMM priors. We should not over interpret these results since a biologist’s interpretation of a clustering algorithm’s output often defines cell-type annotations. The GMM generally uses fewer clusters than the VMM and often fewer than the number of annotated cell types. The VMM uses a reasonable number of clusters and exhibits

Table 3: scRNA-seq clustering performance. We bold top performances using a paired t -test when $p \leq 0.05$.

Dataset	Donors	Cell types	Prior	Utilized clusters	Accuracy	NMI (merged)	NMI (unmerged)
cortex	1	7	GMM	12.4 \pm 1.90	0.791 \pm 0.04	0.648 \pm 0.03	0.637 \pm 0.03
			VMM	15.9 \pm 2.23	0.815 \pm 0.04	0.669 \pm 0.02	0.657 \pm 0.03
pbmc	2	9	GMM	8.9 \pm 1.29	0.706 \pm 0.06	0.778 \pm 0.05	0.774 \pm 0.04
			VMM	10.9 \pm 0.74	0.833 \pm 0.08	0.826 \pm 0.02	0.774 \pm 0.01
lung atlas	16	17	GMM	11.8 \pm 3.08	0.403 \pm 0.10	0.551 \pm 0.05	0.559 \pm 0.04
			VMM	27.6 \pm 4.40	0.552 \pm 0.06	0.632 \pm 0.03	0.654 \pm 0.02
split-seq	2	18	GMM	8.8 \pm 1.32	0.551 \pm 0.11	0.608 \pm 0.04	0.591 \pm 0.03
			VMM	18.9 \pm 2.38	0.747 \pm 0.07	0.698 \pm 0.03	0.630 \pm 0.01

 Table 4: scRNA-seq integration performance. We bold top performances using a paired t -test when $p \leq 0.05$.

Dataset	Model	Metric Type Prior	Aggregate score			Batch correction				Bio conservation					
			Batch correction	Bio conservation	Total	Graph connectivity	KBET	PCR comparison	Silhouette batch	iLISI	Isolated labels	KMeans ARI	KMeans NMI	Silhouette label	cLISI
cortex	scVI tools	$\mathcal{N}(0, I)$	—	0.6712	—	—	—	—	—	0.5669	0.6015	0.5857	0.6066	0.9953	
		$\mathcal{N}(0, I)$	—	0.6607	—	—	—	—	—	0.5707	0.5532	0.5648	0.6182	0.9963	
		GMM	—	0.7145	—	—	—	—	—	0.5887	0.6794	0.6508	0.6548	0.9986	
		VMM	—	0.7337	—	—	—	—	—	0.5904	0.7274	0.6928	0.6594	0.9988	
pbmc	scVI tools	$\mathcal{N}(0, I)$	0.8498	0.6349	0.7208	0.8890	0.9037	0.7532	0.9674	0.7356	0.5742	0.4345	0.5815	0.5855	0.9987
		$\mathcal{N}(0, I)$	0.8679	0.6315	0.7260	0.8887	0.8989	0.8795	0.9592	0.7129	0.5737	0.4129	0.5845	0.5875	0.9988
		GMM	0.8725	0.7318	0.7881	0.8768	0.9006	0.8822	0.9558	0.7470	0.6147	0.6527	0.7268	0.6650	0.9999
		VMM	0.8758	0.7383	0.7933	0.8473	0.8891	0.9361	0.9534	0.7531	0.6167	0.6837	0.7281	0.6630	0.9999
lung atlas	scVI tools	$\mathcal{N}(0, I)$	0.6150	0.5651	0.5850	0.8346	0.3423	0.9323	0.8052	0.6105	0.5720	0.2737	0.4751	0.5289	0.9758
		$\mathcal{N}(0, I)$	0.6159	0.5732	0.5903	0.8431	0.3162	0.9592	0.8195	0.1415	0.5651	0.2919	0.4924	0.5362	0.9801
		GMM	0.5987	0.6095	0.6052	0.8521	0.3712	0.8218	0.8080	0.1404	0.5363	0.3734	0.5789	0.5688	0.9901
		VMM	0.5489	0.6522	0.6109	0.8553	0.4982	0.4790	0.7485	0.1436	0.5150	0.4918	0.6532	0.6121	0.9887
split-seq	scVI tools	$\mathcal{N}(0, I)$	0.8606	0.5670	0.6844	0.8561	0.7106	0.9693	0.9565	0.8106	0.5285	0.2663	0.4994	0.5411	0.9996
		$\mathcal{N}(0, I)$	0.8649	0.5687	0.6872	0.8571	0.7213	0.9776	0.9587	0.8096	0.5267	0.2729	0.5026	0.5417	0.9996
		GMM	0.8741	0.6111	0.7163	0.8574	0.7630	0.9577	0.9557	0.8366	0.5453	0.3400	0.5931	0.5771	0.9999
		VMM	0.8750	0.6244	0.7246	0.8543	0.7635	0.9648	0.9545	0.8381	0.5427	0.3713	0.6191	0.5888	1.0000

accurate clustering performance in most cases, suggesting agreement with the datasets’ manual annotation.

Table 4 compares scRNA-seq integration performances of scVI when using $\mathcal{N}(0, I)$, GMM, and VMM priors on the same battery of metrics that Luecken et al. (2022) use for benchmarking, which they distill into three aggregate scores: “batch correction” assesses the removal of technical variation, “bio conservation” assesses the preservation of biological variation, and “total” is a weighted combination thereof. Batch correction and bio conservation scores are each an average of five different metrics, which we also report. Luecken et al. (2022) scale all metrics to $[0, 1]$ such that bigger values denote better performance. Please see their manuscript for any unfamiliar metric details.

The mouse cortex dataset only has a single batch and thus lacks batch correction scores. For all datasets the VMM has the best bio conservation and total scores. Except for lung atlas, the VMM also has the best batch correction scores. Lung atlas is so named because it has 16 donors and 17 cell types, providing a true atlas-level integration task. Looking at the individual batch correction scores, we find that the PCR (principal component regression) comparison is the metric dragging down the VMM’s batch correction score. This metric measures the relative reduction in total variance explained by the batch variable S for the integrated representation Z w.r.t. the raw count data X :

$$\frac{\text{Var}(X|S) - \text{Var}(Z|S)}{\text{Var}(X|S)}.$$

The score attains its maximal value when $\text{Var}(Z|S) = 0$,

which is an unreasonable expectation for the lung atlas dataset, where donors don’t have cells for every cell type. Therefore, we expect batch ID’s to explain some amount of representation Z . In fact, it is concerning that scVI with a $\mathcal{N}(0, I)$ prior does so well here, suggesting *over* integration. Figure 3 uses MDE to visualize the embeddings and finds that the $\mathcal{N}(0, I)$ prior’s MDE is substantially less structured than that of the VMM, providing an example of MDE benefiting from an already well-structured Z and supporting our case for simultaneous integration and clustering. The GMM’s PCR metric and its qualitative MDE structure lies between those for the $\mathcal{N}(0, I)$ and VMM. We remain cautious of deriving biological insights from an MDE, but using it to qualitatively compare two higher dimensional latent representations is arguably less specious. To our delight, the VMM finds meaningful clusters when comparing the cell-type annotations to VMM cluster assignments (bottom middle and bottom right of Figure 3). Appendix C has MDE comparison plots for the other datasets.

To further confirm the VMM’s batch performance scores on lung atlas were an artifact of having better bio conservation, we use the SPLiT-seq dataset (Shabestari et al., 2022) as a control because every cell is sequenced twice using two slightly different sequencing library preparation steps. Thus, the cells’ biological variability should be identical across the two batches. Indeed, we find the VMM is the top performer on this dataset, allaying concerns it hampered batch correction on the lung atlas data.

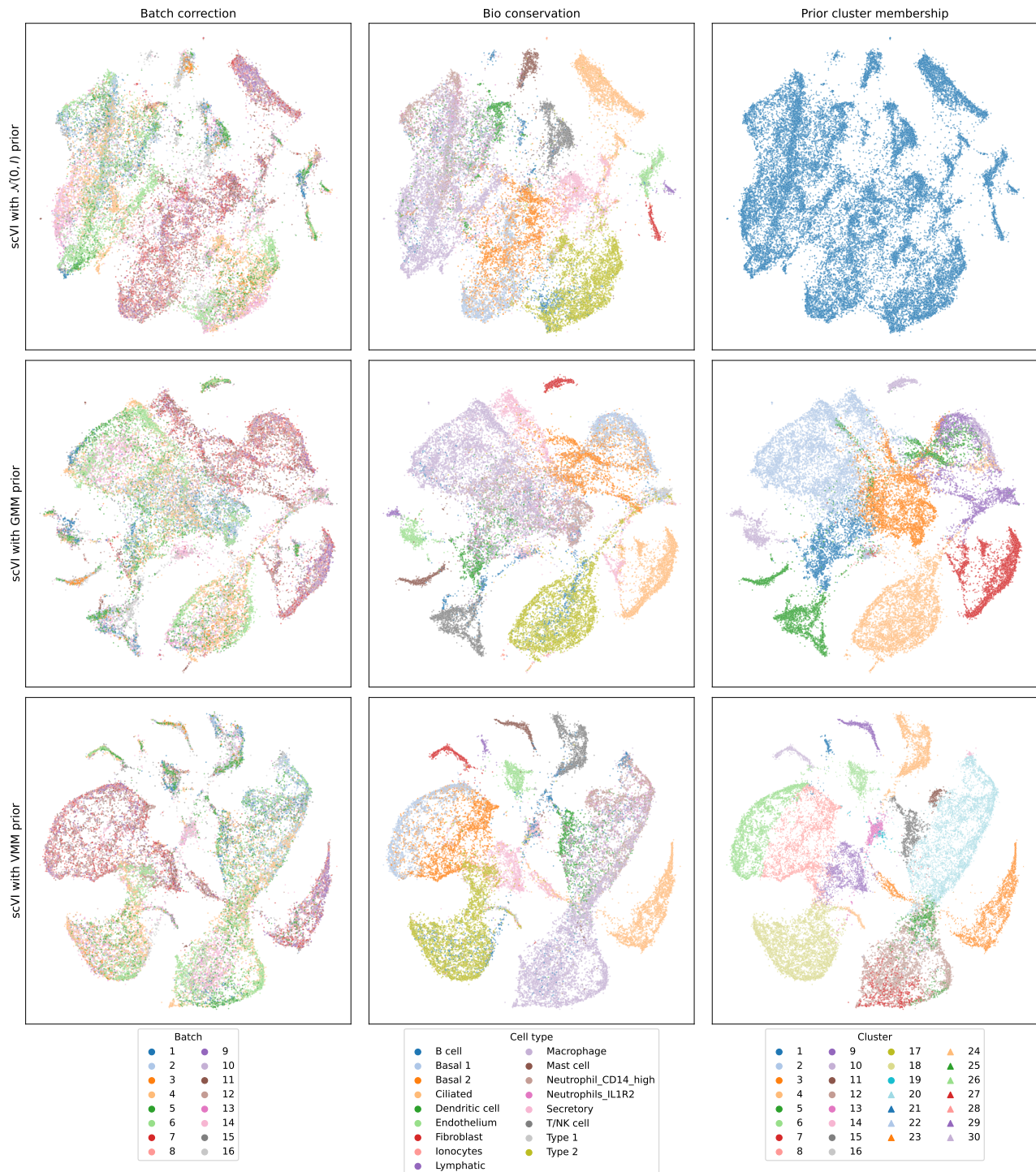


Figure 3: MDE comparison for the lung atlas dataset. Each row has the same embedding across columns for a tested prior. Columns respectively label points by the technical batch identifier, the annotated cell type, and the prior's cluster assignment.

6. Conclusions

Advocating for the simultaneous integration and clustering of scRNA-seq data, we developed the VampPrior Mixture Model (VMM) and an associated inference procedure that are adaptable to *any* DLVM model with continuous latent variables. The VMM produces well-clustered latent representations for both scRNA-seq data and natural images.

The VMM outperforms all VAE-based clustering methods and attains highly competitive image clustering performances relative to all methods. Future work might seek additional performance gains by employing more sophisticated network architectures (e.g. CNNs or transformers).

Replacing scVI's (Lopez et al., 2018) $\mathcal{N}(0, I)$ prior with the VMM significantly elevates its scRNA-seq integration performance, improving both batch correction and biological conservation. The group behind scVI has many popular DLVM-based tools for other biological data modalities, which use $\mathcal{N}(0, I)$ priors in the posited generative processes. We conjecture these methods may derive substantial benefit by replacing the $\mathcal{N}(0, I)$ with our VMM and employing our proposed alternating inference procedure. Furthermore, these methods will inherit the VMM's clustering ability and thereby could find meaningful biological clusters.

Acknowledgements

This material is based upon work supported by the National Science Foundation under Grant No. DBI2146398. Any opinions, findings, and conclusions or recommendations expressed in this material are those of the authors and do not necessarily reflect the views of the National Science Foundation.

Impact Statement

As discussed, this paper has the potential to advance biological data analyses using deep latent variable models. There could be societal consequences of our work, none of which we feel must be specifically highlighted here.

References

- Agrawal, A., Ali, A., and Boyd, S. Minimum-distortion embedding. *Foundations and Trends® in Machine Learning*, 14(3):211–378, 2021. ISSN 1935-8237. Publisher: Now Publishers, Inc.
- Alemi, A., Poole, B., Fischer, I., Dillon, J., Saurous, R. A., and Murphy, K. Fixing a broken ELBO. pp. 159–168. PMLR, 2018. ISBN 2640-3498.
- Burda, Y., Grosse, R., and Salakhutdinov, R. Importance Weighted Autoencoders, November 2016.
- URL <http://arxiv.org/abs/1509.00519>. arXiv:1509.00519 [cs, stat].
- Chari, T. and Pachter, L. The specious art of single-cell genomics. *PLOS Computational Biology*, 19(8):e1011288, August 2023. ISSN 1553-7358. doi: 10.1371/journal.pcbi.1011288. URL <https://journals.plos.org/ploscompbiol/article?id=10.1371/journal.pcbi.1011288>. Publisher: Public Library of Science.
- Dilokthanakul, N., Mediano, P. A., Garnelo, M., Lee, M. C., Salimbeni, H., Arulkumaran, K., and Shanahan, M. Deep unsupervised clustering with gaussian mixture variational autoencoders. *arXiv preprint arXiv:1611.02648*, 2016.
- Edward, R. C. The infinite gaussian mixture model. *Advances in neural information processing systems*, pp. 554–560, 2000.
- Fraley, C. and Raftery, A. E. Bayesian regularization for normal mixture estimation and model-based clustering. *Journal of classification*, 24(2):155–181, 2007. ISSN 0176-4268. Publisher: Springer.
- Hoffman, M. D. and Johnson, M. J. Elbo surgery: yet another way to carve up the variational evidence lower bound. volume 1, 2016. Issue: 2.
- Ishwaran, H. and James, L. F. Approximate Dirichlet Process Computing in Finite Normal Mixtures: Smoothing and Prior Information. *Journal of Computational and Graphical Statistics*, 11(3):508–532, September 2002. ISSN 1061-8600, 1537-2715. doi: 10.1198/106186002411. URL <https://www.tandfonline.com/doi/full/10.1198/106186002411>.
- Jiang, Z., Zheng, Y., Tan, H., Tang, B., and Zhou, H. Variational Deep Embedding: An Unsupervised and Generative Approach to Clustering. In *Proceedings of the Twenty-Sixth International Joint Conference on Artificial Intelligence, IJCAI 2017, Melbourne, Australia, August 19-25, 2017*, pp. 1965–1972, 2017. doi: 10.24963/IJCAI.2017/273. URL <https://doi.org/10.24963/ijcai.2017/273>.
- Johnson, M. J., Duvenaud, D. K., Wiltschko, A., Adams, R. P., and Datta, S. R. Composing graphical models with neural networks for structured representations and fast inference. *Advances in neural information processing systems*, 29, 2016.
- Kingma, D. P. and Ba, J. Adam: A method for stochastic optimization. *arXiv preprint arXiv:1412.6980*, 2014.
- Kingma, D. P. and Welling, M. Auto-encoding variational bayes. *arXiv preprint arXiv:1312.6114*, 2013.

- Korsunsky, I., Millard, N., Fan, J., Slowikowski, K., Zhang, F., Wei, K., Baglaenko, Y., Brenner, M., Loh, P.-r., and Raychaudhuri, S. Fast, sensitive and accurate integration of single-cell data with Harmony. *Nature Methods*, 16(12):1289–1296, December 2019. ISSN 1548-7091, 1548-7105. doi: 10.1038/s41592-019-0619-0. URL <http://www.nature.com/articles/s41592-019-0619-0>.
- Lopez, R., Regier, J., Cole, M. B., Jordan, M. I., and Yosef, N. Deep generative modeling for single-cell transcriptomics. *Nature methods*, 15(12):1053–1058, 2018. ISSN 1548-7091. Publisher: Nature Publishing Group US New York.
- Luecken, M. D., Büttner, M., Chaichoompu, K., Danese, A., Interlandi, M., Müller, M. F., Strobl, D. C., Zappia, L., Dugas, M., and Colomé-Tatché, M. Benchmarking atlas-level data integration in single-cell genomics. *Nature methods*, 19(1):41–50, 2022. ISSN 1548-7091. Publisher: Nature Publishing Group US New York.
- Lähnemann, D., Köster, J., Szczurek, E., McCarthy, D. J., Hicks, S. C., Robinson, M. D., Vallejos, C. A., Campbell, K. R., Beerenwinkel, N., and Mahfouz, A. Eleven grand challenges in single-cell data science. *Genome biology*, 21(1):1–35, 2020. ISSN 1474-760X. Publisher: BioMed Central.
- McInnes, L., Healy, J., and Melville, J. Umap: Uniform manifold approximation and projection for dimension reduction. *arXiv preprint arXiv:1802.03426*, 2018.
- Nalisnick, E., Hertel, L., and Smyth, P. Approximate inference for deep latent gaussian mixtures. volume 2, pp. 131, 2016.
- Nalisnick, E. T. and Smyth, P. Stick-Breaking Variational Autoencoders. In *5th International Conference on Learning Representations, ICLR 2017, Toulon, France, April 24-26, 2017, Conference Track Proceedings*, 2017. URL <https://openreview.net/forum?id=S1jmAotxg>.
- Ranganath, R., Gerrish, S., and Blei, D. Black box variational inference. pp. 814–822. PMLR, 2014.
- Rezende, D. J., Mohamed, S., and Wierstra, D. Stochastic backpropagation and approximate inference in deep generative models. pp. 1278–1286. PMLR, 2014.
- Shabestari, S. K., Morabito, S., Danhash, E. P., McQuade, A., Sanchez, J. R., Miyoshi, E., Chadarevian, J. P., Claes, C., Coburn, M. A., Hasselmann, J., Hidalgo, J., Tran, K. N., Martini, A. C., Rothermich, W. C., Pasqual, J., Head, E., Hume, D. A., Pridans, C., Davtyan, H., Swarup, V., and Burton-Jones, M. Absence of microglia promotes diverse pathologies and early lethality in Alzheimer’s disease mice. *Cell reports*, 39(11):110961, June 2022. ISSN 2211-1247. doi: 10.1016/j.celrep.2022.110961. URL <https://www.ncbi.nlm.nih.gov/pmc/articles/PMC9285116/>.
- Stirm, A., Jebara, T., and Knowles, D. A new distribution on the simplex with auto-encoding applications. *Advances in Neural Information Processing Systems*, 32, 2019.
- Stuart, T., Butler, A., Hoffman, P., Hafemeister, C., Paapeksi, E., Mauck, W. M., Hao, Y., Stoeckius, M., Smibert, P., and Satija, R. Comprehensive Integration of Single-Cell Data. *Cell*, 177(7):1888–1902.e21, June 2019. ISSN 00928674. doi: 10.1016/j.cell.2019.05.031. URL <https://linkinghub.elsevier.com/retrieve/pii/S0092867419305598>.
- Svensson, V., Gayoso, A., Yosef, N., and Pachter, L. Interpretable factor models of single-cell RNA-seq via variational autoencoders. *Bioinformatics*, 36(11):3418–3421, 2020. ISSN 1367-4803. Publisher: Oxford University Press.
- Tomeczak, J. and Welling, M. VAE with a VampPrior. pp. 1214–1223. PMLR, 2018. ISBN 2640-3498.
- Van der Maaten, L. and Hinton, G. Visualizing data using t-SNE. *Journal of machine learning research*, 9(11), 2008. ISSN 1532-4435.
- Williams, R. J. Simple statistical gradient-following algorithms for connectionist reinforcement learning. *Reinforcement learning*, pp. 5–32, 1992. ISSN 1461366089. Publisher: Springer.
- Xu, C., Lopez, R., Mehlman, E., Regier, J., Jordan, M. I., and Yosef, N. Probabilistic harmonization and annotation of single-cell transcriptomics data with deep generative models. *Molecular systems biology*, 17(1):e9620, 2021. ISSN 1744-4292.
- Zhou, S., Xu, H., Zheng, Z., Chen, J., li, Z., Bu, J., Wu, J., Wang, X., Zhu, W., and Ester, M. A Comprehensive Survey on Deep Clustering: Taxonomy, Challenges, and Future Directions, June 2022. URL <http://arxiv.org/abs/2206.07579>. arXiv:2206.07579 [cs].

A. Software Availability

Our code is available at <https://github.com/astirn/VampPrior-Mixture-Model>. We performed all experiments on a laptop with 16GB of RAM connected to an external Nvidia 3090 GPU.

B. VAE Experiments

For all VAE experiments, we use Adam (Kingma & Ba, 2014) with a 1e-4 learning rate. Stochastic gradient ascent's appearance in Algorithm 1 is for illustrative purposes only. Following Jiang et al. (2017), we use ReLU activations for all hidden layers. Please see our provided code for additional implementation details. Figure 4 complements Figure 2 from the main text.

For Table 1, we allow all models to train for a maximum of 500 epochs, but stop training early if the validation set's ELBO has not improved for 20 epochs. For Table 2, we allow all models to train for a maximum of 10,000 epochs, which no model comes close to using since we stop training early if the validation set's unmerged NMI has not improved for 100 epochs. After halting training, we restore the models parameters from the best epoch.

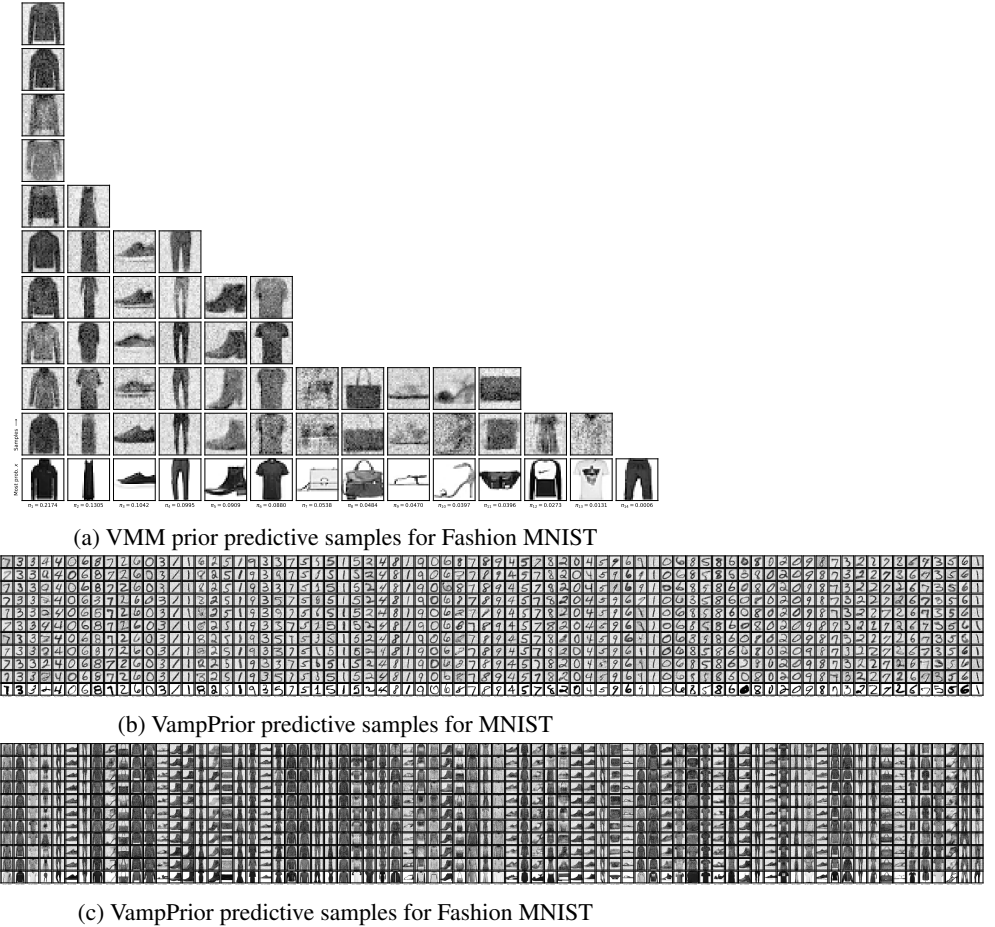


Figure 4: Prior predictive samples. The number of columns equals the number of utilized clusters. The first row shows the data with the highest probability of belonging to the cluster, under which we print the cluster's probability π_j . The rows above are samples from the corresponding component distribution. The number of samples for each component equals $\text{round}(10 \cdot \pi_j / \max(\pi))$. The VampPrior has uniform prior class probabilities since it specifies $\pi_j = K^{-1}$ and does not fit π during inference.

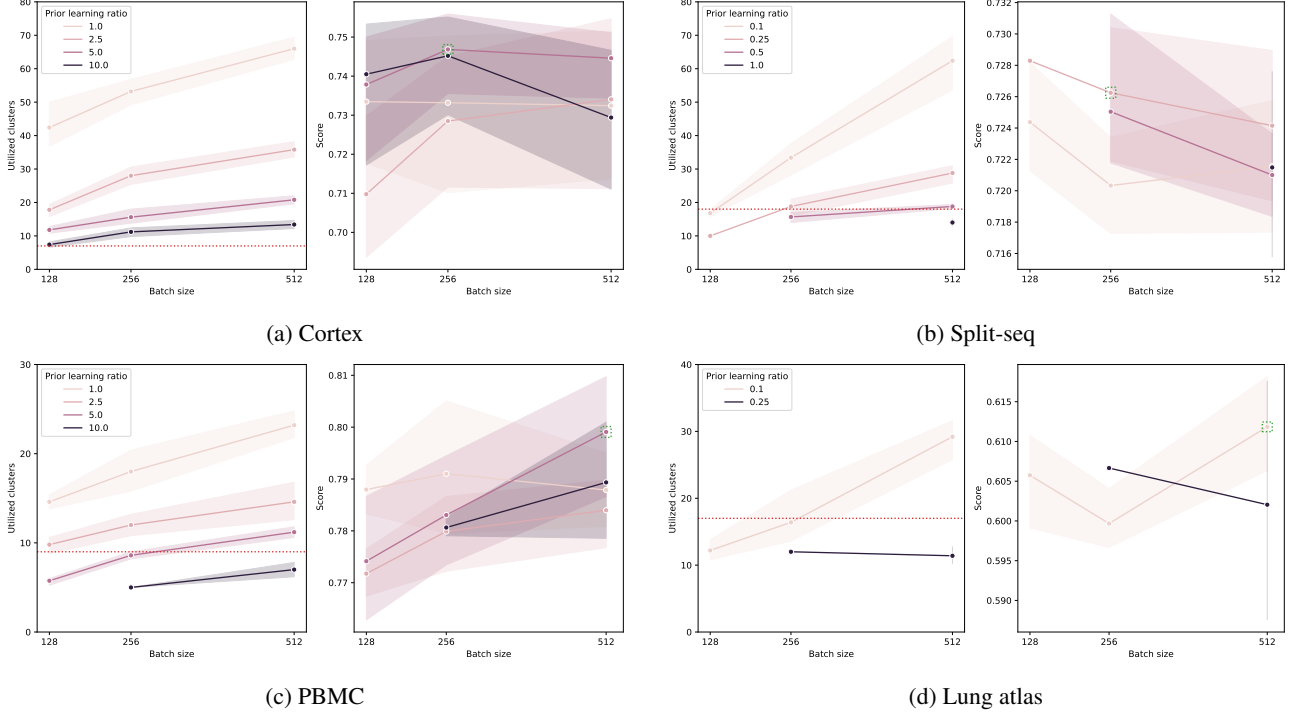


Figure 5: Tuning batch size and prior learning ratio for scVI with a VMM prior. Shading denotes 95% CIs. The left plot shows the number of discovered clusters with a dotted red line indicating the number of unique cell types. The right plot shows the integration score. We place a dotted green box around VMM’s peak performance subject to it discovering an amount of clusters \geq the number of cell types in the dataset.

C. Single Cell Data Analysis

We use Lopez et al. (2018)’s recommended learning rates for scVI’s variational inference steps. However, these learning rates are not always appropriate for our proposed prior inference step when using GMM and VMM priors. Similar to tuning the VAE’s batch size (Figure 1), we tune scVI’s batch size and also a prior learning ratio. For the GMM and VMM, their Empirical Bayes learning rate γ_2 in Algorithm 1 is then VI’s learning rate γ_1 multiplied by this ratio. Figure 5 (analogous to Figure 1) plots the tuning results across a maximum of five trials. Since increasing the prior learning ratio reduces the number of utilized clusters, our tuning loop, for each trial, will advance to the next batch size (beginning with a prior learning ratio of 1.0) whenever the VMM identifies fewer clusters than the number of unique annotated cell types. In selecting the best combination of batch size and prior learning ratio, we maximize Luecken et al. (2022)’s aggregate total score for datasets with multiple batches or the aggregate bio conservation score for datasets with a single batch subject to the number of utilized clusters being \geq the number of cell types in the dataset. Please see our provided code for additional details.

For all scRNA-seq results (Tables 3 and 4 and Figures 3 and 6 to 8), we set $K = 100$ as we did for the VAE and allow all models to train for a maximum of 10,000 epochs. Again, no model comes close to using that many epochs since we halt training early if the validation set’s ELBO has not improved for 100 epochs. We use the ELBO for early stopping in these experiments because the $\mathcal{N}(0, I)$ prior does not perform clustering. As before, we restore the models parameters from the best epoch.

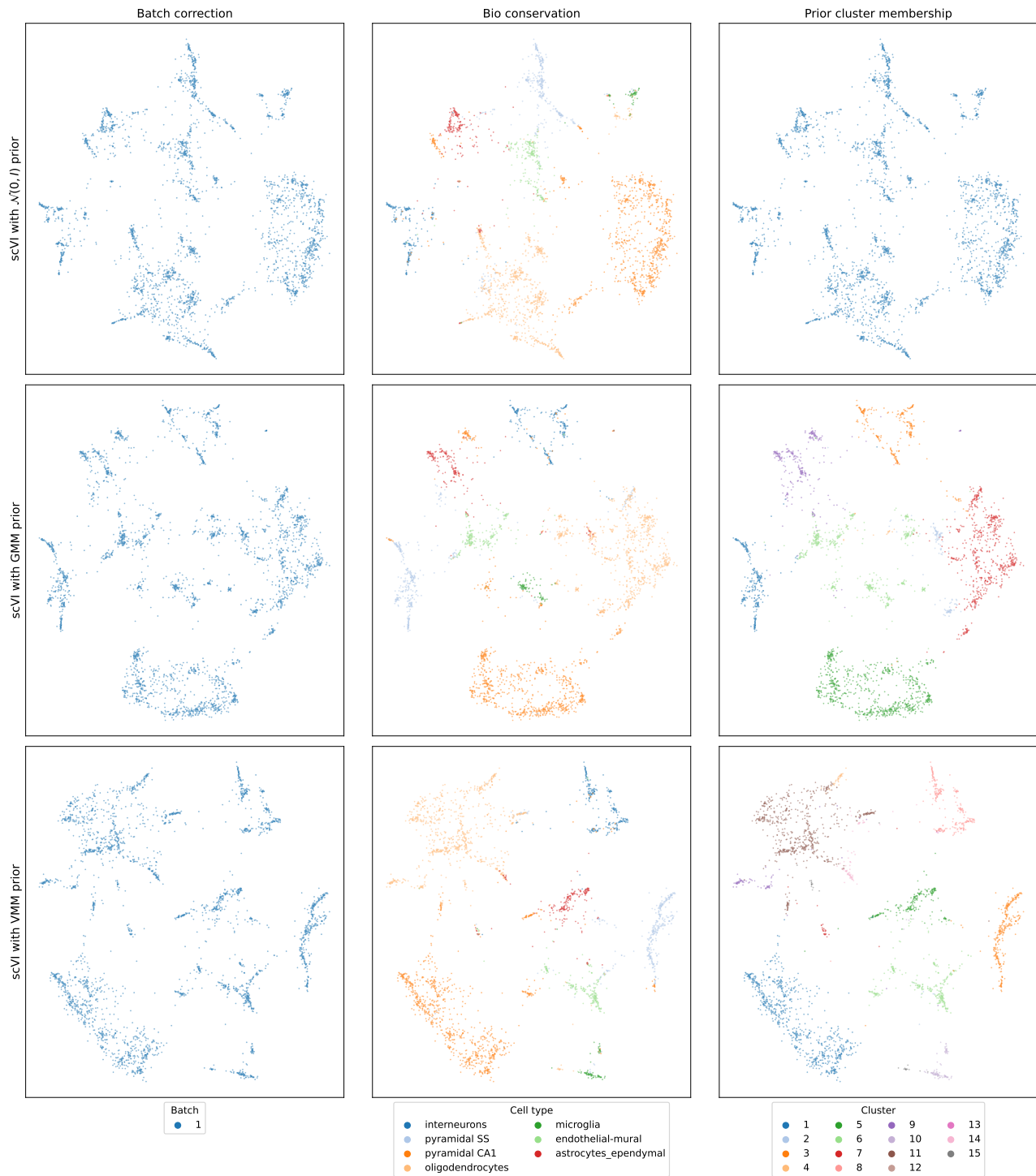


Figure 6: MDE comparison for the cortex dataset. Each row has the same embedding across columns for a tested prior. Columns respectively label points by the technical batch identifier, the annotated cell type, and the prior's cluster assignment.

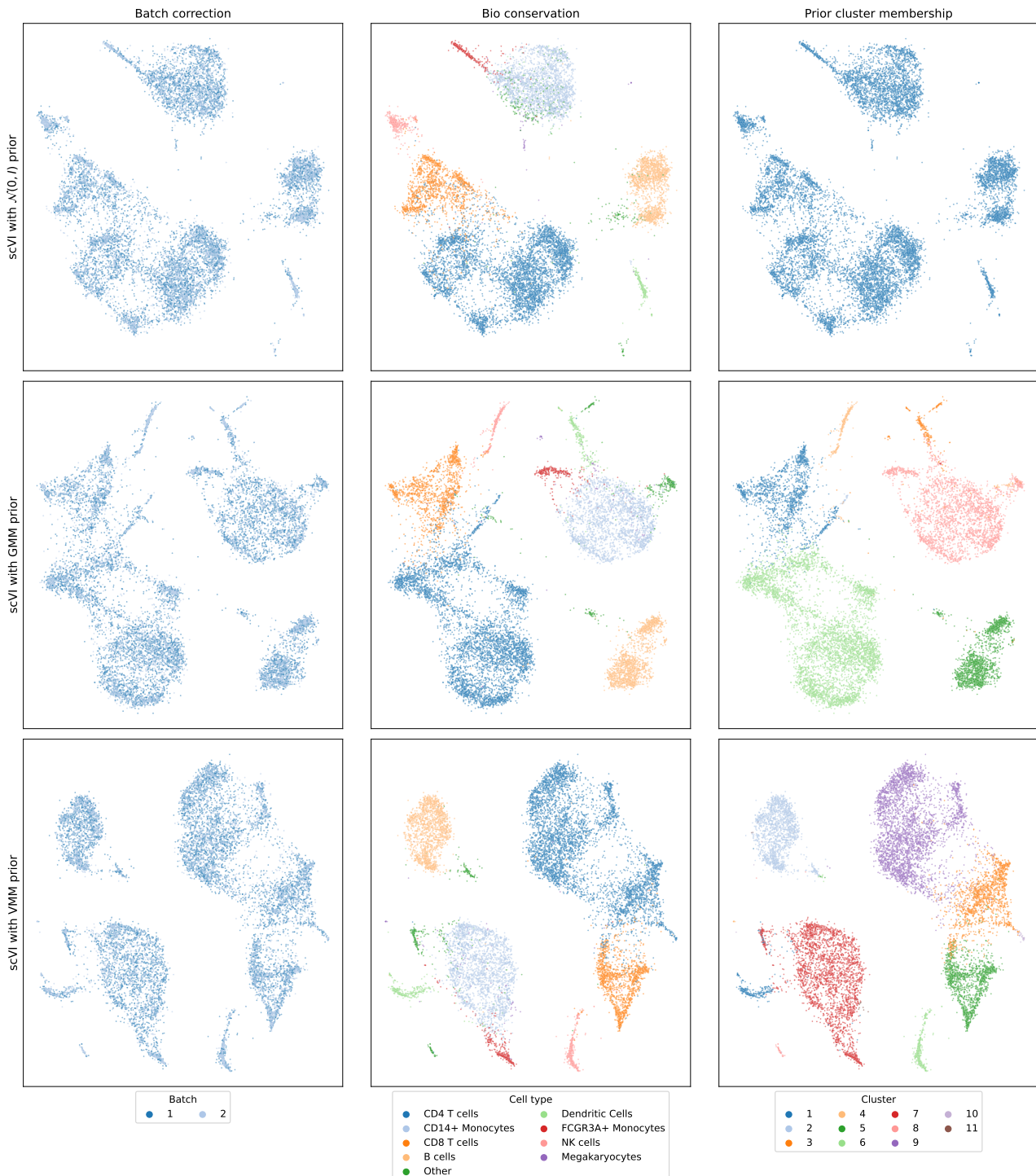


Figure 7: MDE comparison for the PBMC dataset. Each row has the same embedding across columns for a tested prior. Columns respectively label points by the technical batch identifier, the annotated cell type, and the prior's cluster assignment.

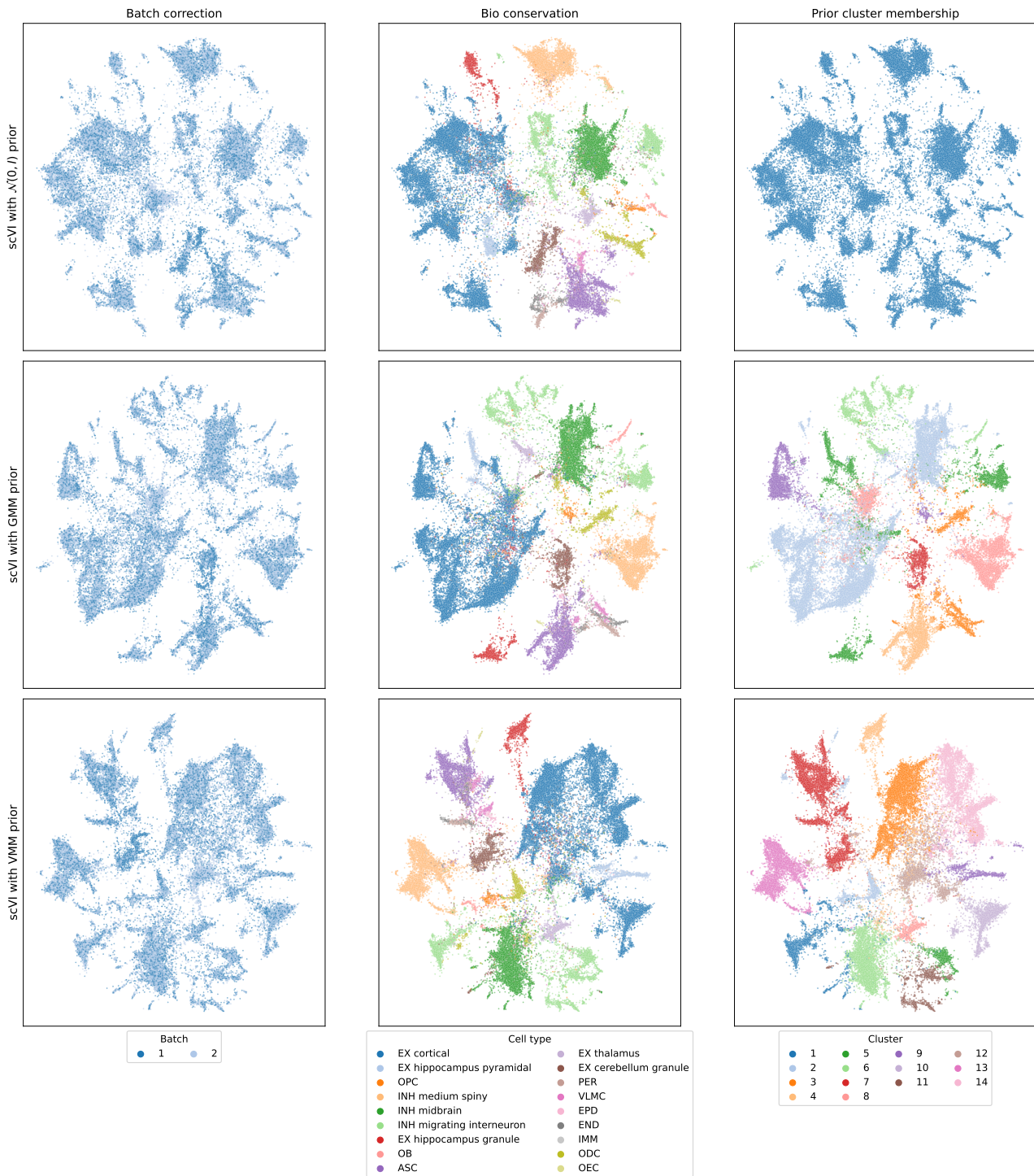


Figure 8: MDE comparison for the split-seq dataset. Each row has the same embedding across columns for a tested prior. Columns respectively label points by the technical batch identifier, the annotated cell type, and the prior's cluster assignment.